Kinetic Investigation by Batch Processing of Film Growth During the Electrodeposition of Titanium from Ethaline

Katarzyna Grubel[1], Diana B. Horangic[1], Steven Livers[1], Christopher J. Chancellor[1], Riah Burnett[2], Bailey Byrd[2], Bethany Lawler[1], Christina Arendt[1], Lance R. Hubbard[1]*

1: PNNL
2: Alabama State University
*: Corresponding Author

Keyword
Deep Eutectic Solvent, Electroplating, Titanium, Electrochemical Impedance Spectroscopy, Cyclic Voltammetry, Large Dataset Processing

Abstract
Titanium electrodeposition as a technological advance has been out of reach due to the poor film quality obtained when using previously developed methods. We have shown that the electrodeposition of Ti is possible and feasible from the deep eutectic solvent (DES) ethaline. Moreover, we have shown through batch analysis that this deposition has temperature-dependent aspects that alter the film deposition kinetics upon modest heating. Our ultraviolet-visible (UV-vis) spectroscopic study has highlighted the more facile reduction of Ti^{4+} to Ti^{3+} and then to Ti^{2+} at elevated temperatures. Understanding the underlying kinetics of electrodeposition will open up new venues for the application of this important metal.

Table of Contents Figure and Text

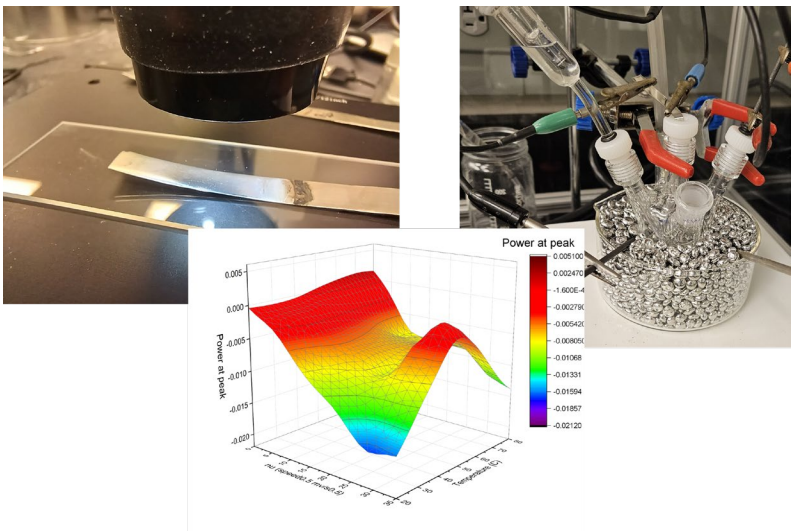

The electrodeposition of titanium in ethaline appears to proceed according to established kinetics in prior literature except above 50°C where the production of intermediary ions from the polyol process begins to play a large role in the deposition kinetics.

Introduction

Titanium electrodeposition as a technological advance has been out of reach due to the poor film quality obtained when using previously developed methods.[1-3] Titanium (Ti) is a refractory metal of crucial importance to medical, automotive, and aerospace industries, deposition of which on various metallic and non-metallic substrates leads to their increased strength, inertness, and corrosion resistance.[4-6] Generally, electroplating has remained out of reach for titanium and similar metals as their reductive bias is greater than the electrolysis bias of water, thus only non-aqueous solutions could be used.

Deep eutectic solvents (DESs), a category of non-aqueous organic solvents, are being intensely investigated for their applicability, usefulness, and low costs.[7, 8] DESs have been previously used for electrodeposition of a multitude of metals and alloys,[9] but to date, there is no report of successful electrodeposition of refractory metals from them. As late as 2017, it was postulated to be nearly impossible to deposit refractory metals such as Ti from ionic liquids (a similar organic solvent).[1, 10] In 2021, it was shown that Ti sheet could be electropolished in the DES ethaline.[11] However, it was long noted in the literature, that while reasonable electrodeposition of titanium can be accomplished in molten salts electrodeposition at near-ambient temperatures almost always led to the deposition of titanium oxides.[10, 12, 13] Thus, the electropolishing result was promising, but more work was needed to demonstrate that ethaline can be an effective solvent for titanium electrodeposition.

Previously, particular steps for Ti(IV) reduction have been proposed based on the electrochemical potentials,[12, 14, 15] but they lacked a secondary method that would confirm the specific suggested sequence. While the mechanism of this deposition can be mostly resolved using reduction potentials, there are no reports supporting an exact layer growth mechanism, that is, whether a monolayer is formed first, or the deposition proceeds through a different pathway such as island growth.

The electrochemical impedance spectroscopy (EIS) technique has been used for the characterization of film deposition processes.[16] It has also been used to ascertain the growth mechanism upon film deposition as well as destruction of the electrodes and electrodeposition.[17-19] It has been shown that EIS is sensitive to the porosity and electrical resistance of the working surface of the electrode.[20]

In this paper, we describe the successful electrodeposition of Ti on a stainless-steel substrate using the DES ethaline. We characterize the electrodeposition film growth kinetics and use optical spectroscopy to evaluate the in-situ presence and identity of titanium ions in the solution. Based on our previous experiences, we initially hypothesized that:
1) Electrodeposition of Ti progresses through the formation of "islands" that then grow to form a complete layer.
2) Electroless polyol reduction of Ti(IV) ions increases the presence of Ti(III) and Ti(II) at temperatures greater than 60^{o}C.

In this study, we have shown that the electrodeposition of Ti is possible and feasible from the DES ethaline. Moreover, we have shown that this deposition has temperature-dependent aspects that alter the film deposition kinetics upon modest heating. Our UV-vis spectroscopic study has highlighted the more facile reduction of Ti^{4+} to Ti^{3+} and then to Ti^{2+} at elevated temperatures.

Experimental

Materials

The chemicals used in the current study are listed in Table 1. All chemicals were used without further purification.

Table 1. List of chemicals used in this study.

Name	CAS	Purity (%)	Supplier
Choline Chloride	67-48-1	98+	ThermoFisher Sci.
Ethylene Glycol	107-21-1	99.8	Acros Organics
Lithium Chloride	7447-41-8	99.98	Sigma Aldrich
Titanium Tetrachloride	7550-45-0	99.9	Acros Organics
Titanium Tetrabromide	7789-68-6	98	Sigma Aldrich
Titanium Tetrafluoride	7783-63-3	98	Alfa Aesar
Isopropyl Alcohol	67-63-0	99.9	Fisher Scientific

Electrochemical Solvent and General Electrical Procedure

Ethaline has been synthesized from choline chloride and ethylene glycol (1:2 molar ratio) by combining them in the inert atmosphere of argon and stirring (300 RPM), and then stored under a slow constant sparge of Ar.

The general procedure for electrochemical experiments: In a 20 mL scintillation vial, 20 mL of DES was combined in the air with lithium chloride (10 mg) and a source of titanium (0.334 g TiF_4, 0.3 mL $TiCl_4$, 0.613 g $TiBr_4$). Solids were added directly into the vial, while $TiCl_4$ was drawn through a 5-micron polyvinyl difluoride (PVDF) membrane syringe filter into a disposable syringe and then discharged into DES solution. Obtained suspensions were put under a blanket of argon and sonicated at 60 °C, resulting in a

clear homogeneous solution. Next, the solution was transferred to a 5-port Gamry Inc. small Dr. Bob's Cell™ and vendor-supplied fittings (https://www.gamry.com/cells-and-accessories/electrochemical-cells/dr-bob-s-cell/). The cell was inserted into a glass bowl with metallic thermal-transfer beads and placed on a hot plate where the temperature was set from 30°C to 90°C during separate runs. Electrochemistry experiments were set up in the cell equipped with a DES-filled glass reference electrode, graphite counter electrode, and stainless-steel (316, McMaster Carr product: 2317K275) working electrode. The working electrode was polished with 400A sandpaper and wiped with a Kimwipe™ immediately before its insertion into the corrosion cell. During electroplating, the reaction was kept under a constant blanket of Ar.

The electrochemical measurements were performed with a Gamry Inc. Interface 1010E potentiostat. Plating occurred by square wave pulse plating of 0.1 s at -1.94 V and 0.05 s at -0.194 vs. Ag/AgCl2 reference (i.e., the rest '0' potential when measured against a standard hydrogen reference electrode). After the electrodeposition experiment was completed, the cathode was removed and rinsed with isopropanol and then submerged and sonicated (40W, 40 kHz) in isopropanol for 5 min. After sonication, the cathode was dried under a light argon stream and placed into a vacuum desiccator until imaging and/or electrical resistance measurements were taken.

Optical Experiments Procedure

Optical experiments were performed in the argon-filled glove bag in a 20 mL scintillation vial equipped with a custom, 3D-printed cap (Figure S1). Background absorption of DES was recorded before each measurement. General procedure: 10 mg of LiCl was weighed into a 20 mL scintillation vial. Next, DES was added, and the vial was blanketed with argon. $TiCl_4$ was drawn through the filter and discharged into the DES solution. The obtained suspension was put under a blanket of argon and sonicated (40 kHz, 40W) at 60 °C, resulting in a clear, homogeneous solution, which was taken directly into the glove bag. Samples were heated to desired temperatures using a hot plate, and the progress of reactions was monitored using an optical exposure chamber. Data was collected using Ocean Optics OceanView software at regular intervals (1 or 60 s).

Measurement and Characterization

Electrochemical measurements were carried out using Gamry E1010B Potentiostat. The specific settings for each measurement are recorded in the data headers; example data headers for each electrochemical measurement type are provided in the supplemental information. Electrical resistance evaluation of the plated films and reference standards was accomplished with a Keysight B258A electrometer and vendor-supplied tri-ax cabling and alligator clips.

Scanning electron microscopy (SEM) was performed using a JEOL IT-800 Field Emission Scanning Electron Microscope, coupled with an Oxford 80 X-Max energy dispersive spectrometer (EDS). Variable accelerating voltages ranging from 5 to 30 kV were used. Scanning transmission electron microscopy (STEM) was done on a JEOL JEM-ARM200CF ACCELARM spherical aberration corrected (Cs) microscope operated at 200 kV using a JEOL Centurio SSD-EDS detector with a solid collection angle of 0.9 sr.

X-ray fluorescence was measured with a Bruker Scientific S2 PICOFOX total reflection X-ray fluorescence (TXRF) spectrometer. Custom acrylonitrile butadiene styrene (ABS) printed dishes were used to hold the coupons in the TXRF. All samples were measured for 1 hr with a molybdenum cathode and a nominal current of 60 microamps. All data was normalized to the intensity of the iron response to allow for comparison between samples.

Optical ultraviolet-visible (UV-vis) absorbance data was recorded with an Ocean Optics OCEAN HDX spectrometer with vendor-supplied fused silica optics and cables. All Ocean Insights products were selected for maximum light collection from 195-850 nm. The optical cell was purchased from Thor Labs Inc. (model CVH100) and connected via SubMiniature A (SMA) collimating lenses with fused silica optics (models CVH100-COL, LA4647).

Data Analysis

Optical/SEM images were analyzed with Image J v1.53. Electrochemical data (excluding cyclic voltammetry) was analyzed with Gamry's EChem Analyst software.
Collected cyclic voltammetry (CV) data was analyzed using a custom-developed algorithm for batch processing of electrochemical data[21]. The analysis methodology is contained in the supplement information. X-ray fluorescence (XRF) data was analyzed using Bruker's PICOFOX control/analysis software. Optical emission data was analyzed with Microsoft Excel after being recorded by Ocean Optics' OceanView control software.

Results

Initial Evaluation

During electrodeposition of titanium on steel, two reduction responses were seen as evidenced by cyclic voltammetry (Figure 1a). The deposition was then analyzed by square wave voltammetry to confirm the reduction biases with minimized capacitance. The reductions appear to be centered around -0.8 V and -1.6 V (adjusted to be *vs.* a standard hydrogen electrode [SHE]) as shown in Figure 1b. The initial reduction response (-0.8 V) occured over a very broad bias range, warranting further investigation. Cyclic voltammetry of both responses was conducted from 10 to 10k mV/s scan speeds with the cell providing ion transfer data from 10 to 1k mV/s. The higher scan speeds had non-linearities as shown in Figure 1c. The center of the reduction biases was plotted against the root of the scan speed to evaluate the diffusive nature of the reduction. As shown in Figure 1d, the reduction to metal occurring at -1. 6 V is linear, while the

intermediary reduction response (-0.8 V) has non-linear aspects at higher scan speeds. Obtained samples were then imaged and chemically analyzed to verify that deposition was taking place.

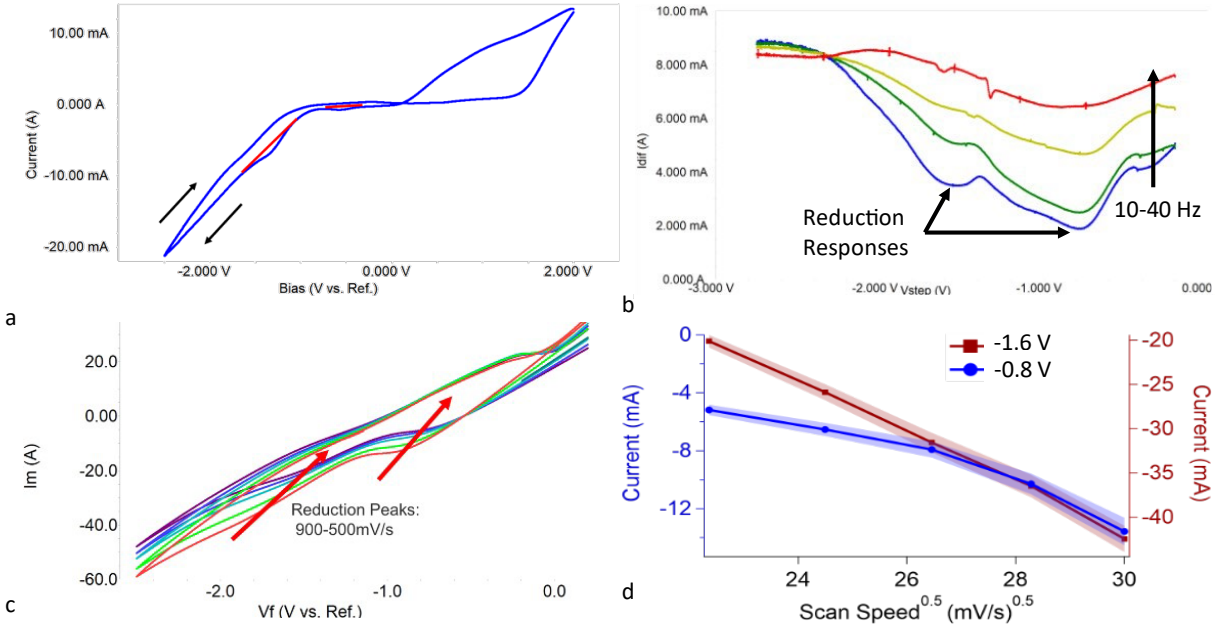

Figure 1. a) Example cyclic voltammogram with the regions of titanium reduction denoted by red lines. b) square wave voltammograms taken with scan speeds from 10-40 Hz. Responses from the two observed reductive reactions are demarked. c) Scan speed comparison of cyclic voltammograms from 500-900 mV/s. d) A plot of the centers of the reduction responses in Figure 1c showing a linear trend from the response occurring at about -1.64 V (red) and a non-linear influence in the response occurring at -0.8 V (blue).

Imaging and Chemical Analysis

Optically, at near-ambient temperatures, the evolution of the titanium deposition appears to happen by island growth on the seconds time scale with full film evolution proceeding after that, as shown in Figure 2a, top panel (30°C). At higher temperatures, the island growth mechanism appears to be supplanted by a conformal layer-by-layer deposition, as shown in Figure 2a, lower panel (95°C). To evaluate this, the films were cross sectioned for scanning electron analysis.

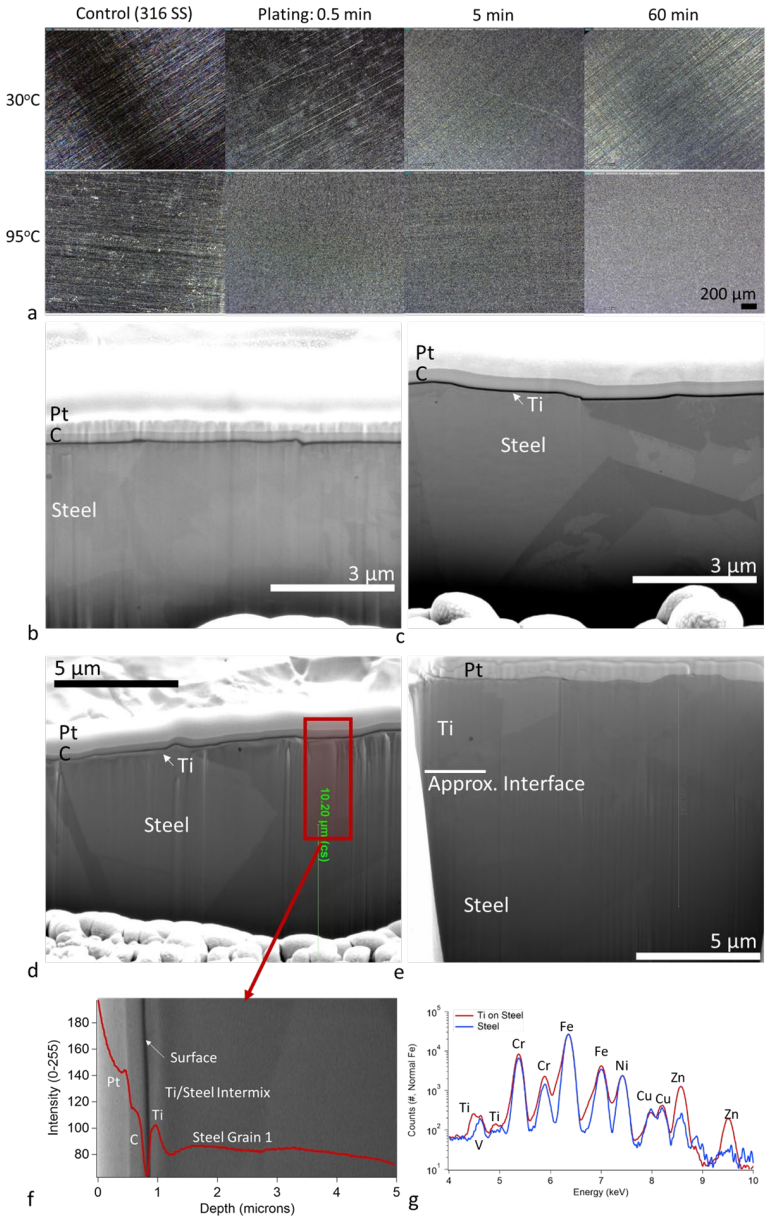

Figure 2. a) Optical image set of the film evolution with temperature and deposition time. b) 20kX SEM cross section of the steel substrate. c) 20 kX SEM cross section of the titanium deposition after 30 s of deposition and at 30°C. d) 35kX SEM cross section of the titanium deposition after 5 min. of deposition and at 90°C. e) 35 kX SEM cross section of the titanium deposition after 1 hr of deposition and at 90°C. f) Intensity analysis of the 5 min plated cross section (with the area marked in Figure 2d), with a 50kX SEM background inset for layer perspective. Each layer is defined by image intensity. g) XRF analysis of the 1 hr plated sample vs. a steel control.

Figure 2b shows steel with caps of carbon and platinum used to illuminate the surface. After 30 s of electroplating the surface appears rougher, which may indicate the presence of islands of titanium (see Figure 2c). After 5 min of plating, a several hundred nanometer-thick conformal film is developing on the surface, which is shown in Figure 2d. The intensity analysis of the cross section allowed for the conformation that the

titanium is forming on the surface, seen in Figure 2f. After 1 hour of deposition, the film is about 3-3.5 microns thick with small grains evident at the boundary between the steel and titanium (see Figure 2e). Lastly, XRF was used to determine the composition of the film, with titanium appearing to be the only addition when compared to a control signal (see Figure 2g). The micron-scale thick films shown in Figure 2e and Figure 2g were also tested for electrical resistance against titanium and steel reference sheets of similar roughness. The electrodeposited films had resistances in line with those of the titanium sheet standard (about 50% less resistance than the steel substrate used for plating).

EIS

To explore the different film depositions seen in Figure 2a, potentiostatic EIS was carried out at two temperatures, three bath compositions, and three different time lengths. Each of the experiments began with a recording of the EIS of the steel electrode before applying current. At low temperatures, the EIS of the SS substrate exhibits an open-loop feature that allows for distinguishing the kinetic control region and mass transfer-controlled region (see Figure 3a). However, at an elevated temperature of 90°C, even before the current is passed through the sample, the appearance of the inductive loop can be seen, indicating that electrode surface modification starts to take place (see Figure 3a).

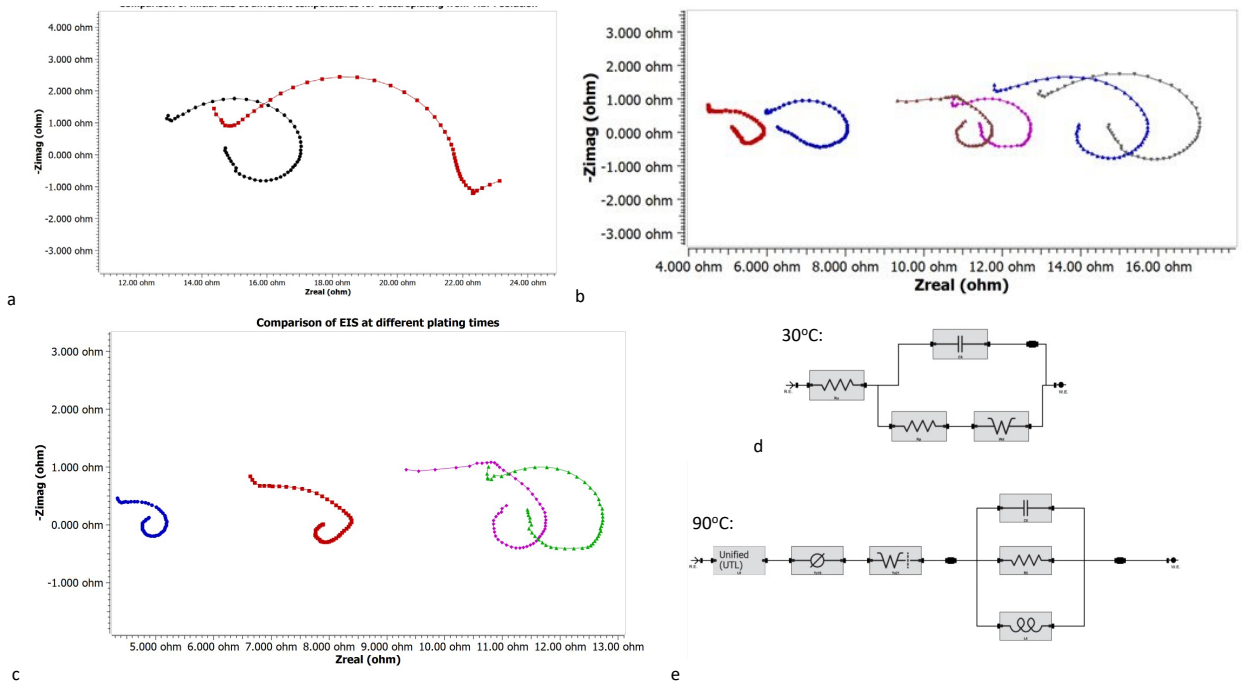

Figure **3.** a) Comparison of the initial EIS between 30°C (red) and 90°C (black) for electroplating solutions of $TiBr_4$ of the same concentration. b) Comparison of Ohmic resistance of Ti coat electrodeposited for 30 sec from different plating baths at 90°C: TiF_4 salt (●start, ■stop), $TiCl_4$ salt (◆start, ▲stop), $TiBr_4$ salt (▼ start, ▲stop). c) Comparison of Ohmic resistance of Ti coat electrodeposited for different periods from the $TiCl_4$ salt at 80 °C (▲ 0 sec., ◆ 30 sec., ■ 5 min., ● 1 h). d) example of simple EIS fitting circuit diagram. e) EIS circuit diagram used to fit EIS post-Ti layer formation.

To better understand the reason for the emergence of the inductive loop (and subsequent alteration in film deposition kinetics), we investigated the influence of different anions on the mechanism of Ti electrodeposition Figure 3b. In each case, the inductive mechanism was shown to be temperature and not ion dependent. In each case, initial EIS recorded at 30°C showed a typical open curve with a clearly distinguishable Warburg region (circuit diagram shown in Figure 3d), but at 90°C, even initial EIS already shows inductive behavior, as evidenced in Figure 3c with corresponding circuit diagram shown in Figure 3e. Further attempts at understanding the non-linearity in the reduction currents seen in Figure 1d were then undertaken.

Cyclic Voltammetry

To better understand the reduction kinetics, a data set of over 1000 cyclic voltammetry scans was taken at varying temperatures (25-90^{o}C) and scan speeds (10-1000 mV/s) for the bath with saturated titanium (IV) chloride. The responses were analyzed for the magnitude of the charge transferred during reduction as well as the maximum magnitude of the reductive current, as shown in Figure 4.

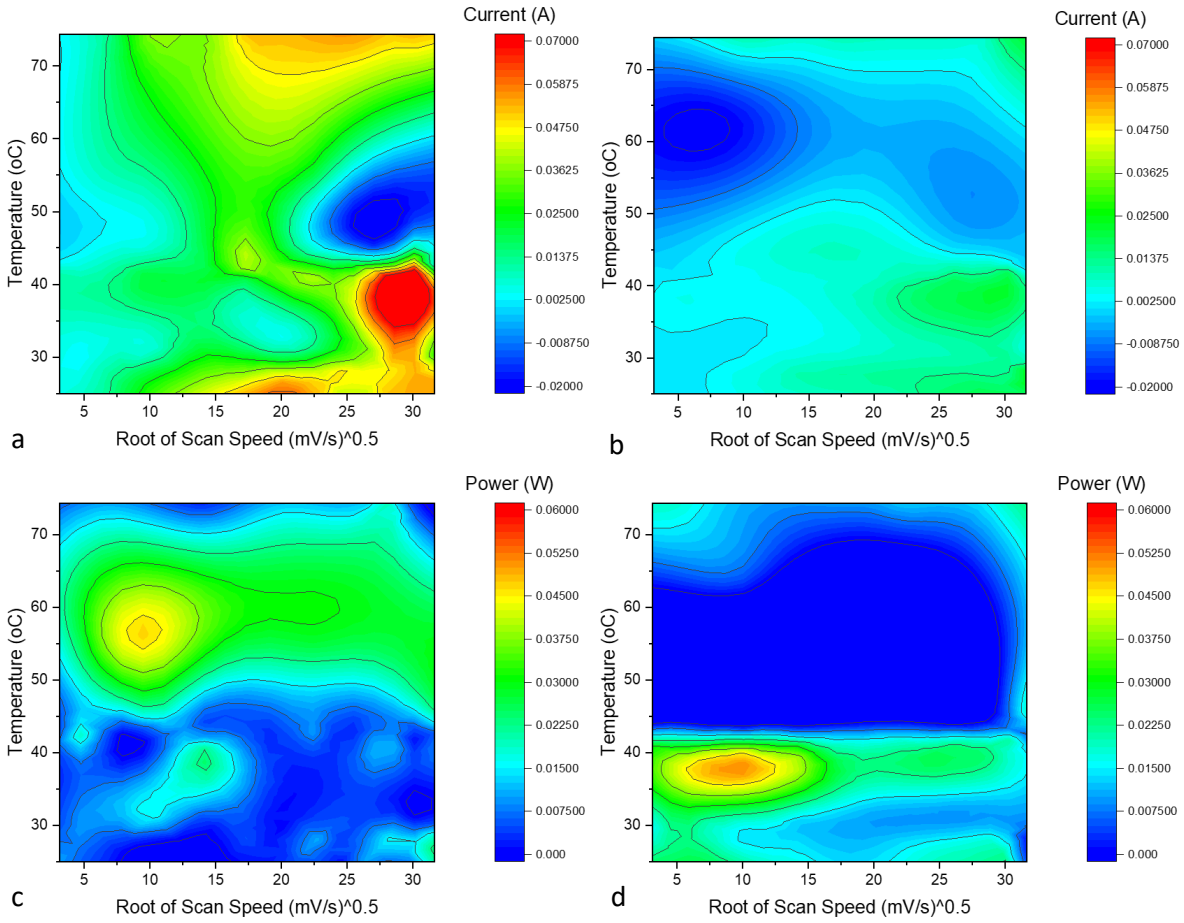

Figure 4. Batch investigation of the cyclic voltammetry of the reduction to titanium (IV) chloride. a) A color map denoting the magnitude of the reductive current for the response occurring at about -0.8 V vs. a standard hydrogen electrode (SHE) taken at various temperatures and scan speeds. b) A color map denoting the magnitude of the reductive current for the response occurring at about -1.6 V vs. SHE taken at various temperatures and scan speeds. c) A color map denoting the magnitude of the integrated charge transfer for the response occurring at about -0.8 V vs. SHE taken at various temperatures and scan speeds. d) A color map denoting the magnitude of the integrated charge transfer for the response occurring at about -1.6 V vs. SHE taken at various temperatures and scan speeds.

The reductive current change of the initial reductive response is linear for slower scan speeds (5-15 $mV^{0.5}/s^{0.5}$), as seen in Figure 4a. Also in Figure 4a, higher scan speeds cause non-linearities to occur (diffusion is no longer the limiting kinetic step). A similar trend is seen in the reductive current of the -1.6 V response seen in Figure 4b. This is true except for one location with higher scan speeds and temperatures from 50 °C -60°C, where both reductive currents are lower than would be expected (see Figures 4a and b).

The total dissipated power (integrated response minus the background signal) of both reductive biases helps explain the trend seen in Figures 4a and b. The power dissipated by the initial reduction at -0.8V is relatively steady with a maximum response of around 60°C (see Figure 4c). Lower temperatures produce less of a response than higher ones as would be expected until an optimal plating temperature is reached.

The reduction of Ti^{2+} to metal at -1.6 V shows a different trend, with its optimal temperature occurring around 40°C and an unexpected dearth of signal at higher temperatures, as seen by the large blue region of Figure 4d. This trend is unexpected, as it was hypothesized that the metal reduction would follow a similar trend of an optimal plating temperature being around 60°C, with slower pulses producing the optimal reductive environment. Since the solvent is relatively transparent across the near-ultraviolet to near-infrared wavelengths and titanium ions have different absorbances in this range, an *in-situ* optical absorption spectroscopy combined with the electrochemical process was undertaken to better understand the unexpected CV results of the metal reduction.

Optical Results

To better understand the impact of solvents on the presence and stabilization of titanium ions in the bath, the optical response of each ion was measured with and without the electrochemical pulse plating and at 60°C, as seen in Figures 5a and 5b. It should be noted that in the ultraviolet to near-infrared range, only Ti^{3+} and Ti^{2+} have unique absorbances that cannot be attributed to other ions.[22-24] Generally, the presence of both intermediary ions is higher during the hot electroplating case as compared to the thermal process only. It should be noted that the Ti^{2+} ion is ever-increasing in concentration during the electroplating case, suggesting that there may be other production means for this intermediary ion.

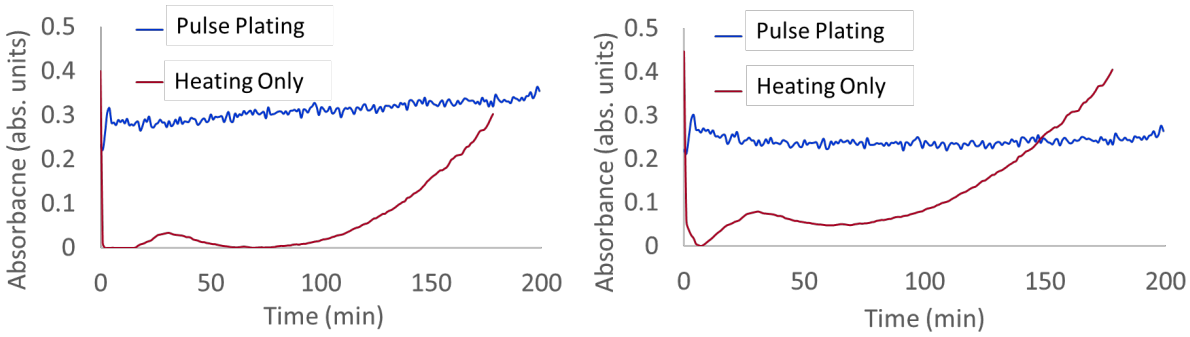

Figure 5. a) A plot of the optical absorbance of 410 nm light, related to the concentration of Ti^{2+} with and without electroplating at 80°C. b) A plot of the optical absorbance of 520 nm light, related to the concentration of Ti^{3+}, with and without electroplating at 80°C.

In Figures 5a and b for the thermal-only cases, the presence of both intermediary ions increases in the solution with time at temperature, with Ti^{3+} being more prevalent overall at all times. It is expected, as it requires the addition of just 1 electron to Ti $^{3+}$ *vs.* 2 electrons for reduction to Ti^{2+}. For the pulse plating at temperature, the presence of

Ti^{2+} is marginally higher and increasing on the minute time scales while the presence of Ti^{3+} remains constant.

Discussion

At temperatures above 60°C, the EIS shows only layer-by-layer growth through a diffusive plane (Figures 3b, c, and e). rather than one reliant on island growth (Figures 3a and d). This switch is partially explained by the presence of non-linear influences in the cyclic voltammetry of the reductive response centered at about -0.8V, seen in Figure 4a. Additionally, based on the EIS result, the initial presence of an inductive loop is evidence of the change in film growth kinetics. It has been shown that for a simple solid electrode (i.e., the metal surface before/during island formation), the impedance of the system should be able to be represented by a simple equivalent circuit with a resistor, capacitor, and Warburg impedance element (accounting for the diffusion-controlled process), as seen in Figure 3d.[25, 26] This solid electrode kinetic model fits the deposition kinetics of ambient temperature electroplating. However, while using our setup and heating it above 60 °C, we have found that we had to account for the inductive loop, as well as the presence of the porous electrodes. The modeling of the inductive loop and porous electrodes in the diagram in Figure 3e is needed as the deposition kinetics change to a layer-by-layer model with the reduction of some ions occurring in narrow pores as the films complete deposition. The use of the united transmission lines (UTLs) accounts for the rate of kinetic reaction in narrow pores of the electrode. The evident change in deposition kinetics is reflected in the optical and electrochemical behavior of the cell.

At temperatures above 60°C, there is an increase in the current which does not align with a linear trend that would be expected from a diffusion-limited process, such as is seen by the mostly linear evolution of the metal reduction response in Figure 1c to d, and Figure 4b. The thermally-dependent non-linearities of the initial reduction response's cyclic voltammetry suggest that it is influenced by the production of ions that are not being driven by electroreduction.

UV-vis assessment during the heating of the solution (Figure 5) shows that if no pulse plating is applied, the presence of both intermediate ions (Ti^{3+} and Ti^{2+}) increases with time. This is suspected to be due to the polyol reduction (Larcher & Patrice, 2000), as the main component of the solvent is ethylene glycol. This assessment is corroborated by the batch analysis of the cyclic voltammetry, which shows non-linear aspects in current for both reduction peaks, with a particular increase evident for the primary reduction bias (-0.8V, Figure 4a and b). It should be noted that the presence of electroplating sequence increases the concentration of both intermediate ions, thus part of their kinetics is driven by electroreduction. Lastly, an important aspect of the optical signature of the intermediate ions is that while the presence of Ti^{3+} remains relatively stable on the minutes time scale (Figure 5b), the presence of Ti^{2+} increases

slightly during pulse plating (Figure 5a). Thus, with the presence of thermal and electrical reduction, there is an overabundance of Ti^{2+} in the bath and available for metal film formation.

The increasing concentration of Ti^{2+} in the bath originating from both electroreduction and solvent-based polyol reduction appears to be the mechanism by which the film growth kinetics change upon heating, as seen in Figure 2a and Figures 3a, c. In ambient electroplating approaches, there would be a dearth of available ions for metal reduction, meaning that the electrochemical cell must provide all the power (as seen by the increased dissipated power in the lower left-hand corner of the heat map in Figure 4d). Film growth would then naturally proceed from ideal plating locations (islands).

Taken together, our observations corroborate the hypothesis that the polyol reduction mechanism is influencing the electrodeposition kinetics at temperatures above 60°C. With an increase in temperature the concentration of the available Ti^{2+} eventually becomes more than what can diffuse to the surface (i.e., the concentration increases in the bath), thus plating occurs in a more layer-by-layer fashion, as is seen in the film depositions at higher temperatures in Figures 2a,c-f and by EIS at higher temperatures, Figures 3b, c, e). Thus, the polyol-induced production of intermediate ions produces a change in the film growth kinetics that is thermally dependent (as the electroless polyol reduction kinetics are). What this means from the perspective of prior literature is that the multi-kinetic route has an increased percentage of Ti^{4+} to Ti^{3+} and Ti^{3+} to Ti^{2+} production.[14] What is not seen is an increase of metal reduction, which optically would be represented as a diminishing concentration evolution with time of the Ti^{2+} absorbance. It appears that the polyol mechanism can enhance the production of intermediate ions but cannot reduce them to elemental metal, which remains a function of the electrochemical process.

Conclusions

The electroreduction of titanium has been challenging to implement in the past. In this publication, we have shown that the electrodeposition of Ti on stainless-steel substrates is feasible from an inexpensive DES solvent ethaline. The reduction kinetics are in line with prior literature at ambient temperatures. Upon modest heating, the influence of the electroless polyol reduction mechanism increases the concentration of intermediate ions, altering the film growth kinetics to a more layer-by-layer method. We have highlighted the importance of temperature control on the reaction and have proposed an electrodeposition mechanism that is supported by multiple analytical methods, such as EIS, UV-vis, and SEM. Our work therefore may open a pathway to simpler and environmentally friendly formation of Ti deposits and alloys for use in critical industries and consumer goods. A methodology to electrodeposit active metals such as titanium can revolutionize medical implants, aerospace, and corrosion barriers, providing a way to combine the mechanical properties of the underlying metal with the anticorrosive properties of the active metals.

References

[1] F. Endres, S. Zein El Abedin, A. Y. Saad, E. M. Moustafa, N. Borissenko, W. E. Price, G. G. Wallace, D. R. MacFarlane, P. J. Newman, A. Bund, *Physical Chemistry Chemical Physics* **2008**, *10*, 2189-2199, https://10.1039/B800353J.

[2] S. Wang, Y. Li, *Journal of Electroanalytical Chemistry* **2004**, *571*, 37-42, https://10.1016/j.jelechem.2004.04.010.

[3] X. Zhang, J. Huang, D. Min, T. Wen, Z. Shi, S. Yang, *International Journal of Hydrogen Energy* **2022**, *47*, 6544-6551, https://10.1016/j.ijhydene.2021.12.038.

[4] L. Hubbard, C. Arendt, R. Webster, Composition and method embodiments for plating metal coatings. US20200378027A1, **2020.** https://patents.google.com/patent/US20200378027A1/en.

[5] V. M. Voyevodin, V. I. Zmii, S. G. Rudenkyi, *Powder Metallurgy and Metal Ceramics* **2017**, *56*, 198-209, https://10.1007/s11106-017-9887-3.

[6] K. O. Legg, M. Graham, P. Chang, F. Rastagar, A. Gonzales, B. Sartwell, *Surface and Coatings Technology* **1996**, *81*, 99-105, https://10.1016/0257-8972(95)02653-3.

[7] H. J. Hayler, S. Perkin, *Chemical Communications* **2022**, *58*, 12728-12731, https://10.1039/D2CC04008E.

[8] H. Moradi, N. Farzi, *Journal of Molecular Liquids* **2021**, *339*, 116669, https://10.1016/j.molliq.2021.116669.

[9] A. P. Abbott, A. Ballantyne, R. C. Harris, J. A. Juma, K. S. Ryder, *Physical Chemistry Chemical Physics* **2017**, *19*, 3219-3231, https://10.1039/C6CP08720E.

[10] C. Xu, Y. Liu, Y. Hua, J. Li, Q. Zhang, *Materials Transactions* **2017**, *58*, 377-382, https://10.2320/matertrans.MK201612.

[11] W. O. Karim, *Arabian Journal of Chemistry* **2021**, *14*, 102906, https://10.1016/j.arabjc.2020.11.012.

[12] B. J. Fortin, J. G. Wurm, L. Gravel, R. J. A. Potvin, *Journal of The Electrochemical Society* **1959**, *106*, 428, https://10.1149/1.2427373.

[13] P. L. Sibrell, *Electrochemical reduction of titanium in nonaqueous solvents*, 9592, United States Bureau of Mines, Reno, NV **1995**.

[14] A. Girginov, T. Z. Tzvetkoff, M. Bojinov, *Journal of Applied Electrochemistry* **1995**, *25*, 993-1003, https://10.1007/BF00241947.

[15] C. Guang-Sen, M. Okido, T. Oki, *Journal of Applied Electrochemistry* **1987**, *17*, 849-856, https://10.1007/BF01007823.

[16] X. Li, R. Deng, Q. Zhang, *Surface and Coatings Technology* **2022**, *443*, 128610, https://10.1016/j.surfcoat.2022.128610.

[17] H. Brandstätter, I. Hanzu, M. Wilkening, *Electrochimica Acta* **2016**, *207*, 218-223, https://10.1016/j.electacta.2016.03.126.

[18] R. Wiart, *Electrochimica Acta* **1990**, *35*, 1587-1593, https://10.1016/0013-4686(90)80014-F.

[19] M. A. Zabara, G. Katırcı, B. Ülgüt, *The Journal of Physical Chemistry C* **2022**, *126*, 10968-10976, https://10.1021/acs.jpcc.2c02396.
[20] N. O. Laschuk, E. B. Easton, O. V. Zenkina, *RSC Advances* **2021**, *11*, 27925-27936, https://10.1039/D1RA03785D.
[21] D. Horangic, L. Hubbard, K. Grubel, **2024**, https://doi.org/10.11578/dc.20250224.2.
[22] D. Aurbach, Y. Gofer, O. Chusid, H. Eshel, *Electrochimica Acta* **2007**, *52*, 2097-2101, https://10.1016/j.electacta.2006.08.019.
[23] D. M. Gruen, D. H. W. Carstens, *The Journal of Chemical Physics* **1971**, *54*, 5206-5214, https://10.1063/1.1674816.
[24] N. R. Mucha, J. Som, S. Shaji, S. Fialkova, P. R. Apte, B. Balasubramanian, J. E. Shield, M. Anderson, D. Kumar, *Journal of Materials Science* **2020**, *55*, 5123-5134, https://10.1007/s10853-019-04278-x.
[25] N. T. C. Oliveira, A. C. Guastaldi, *Acta Biomaterialia* **2009**, *5*, 399-405, https://10.1016/j.actbio.2008.07.010.
[26] G. Saravanan, S. Mohan, *International Journal of Electrochemical Science* **2011**, *6*, 1468-1478, https://10.1016/S1452-3981(23)15086-3.

Supplemental Information

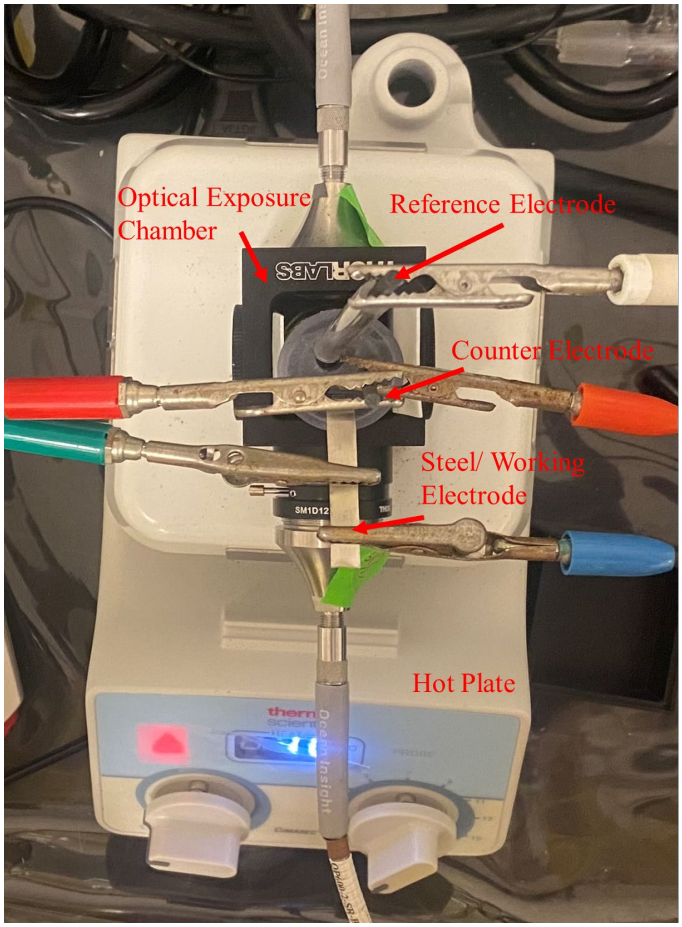

Figure S1. Diagram of the optical and electronic cell used for in-situ optical measurements.

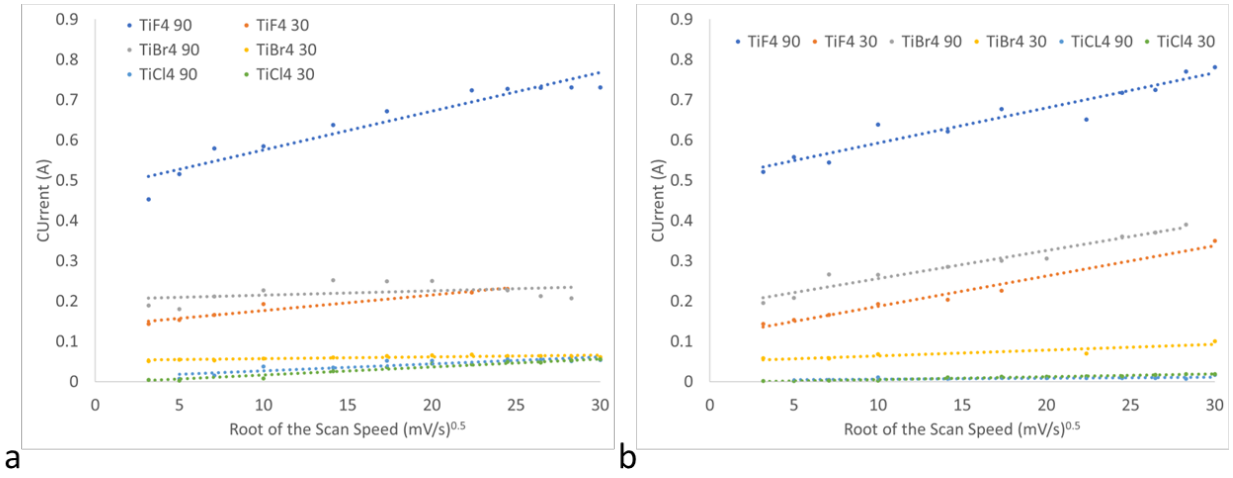

Figure S2. a) Current plotted vs. root of the scan speed for 3 ions of titanium and at 2 temperatures for the reduction current at -0.8V vs. SHE. b) Current plotted vs. the root of the scan speed for 3 counter ions of titanium (IV) and at 2 temperatures for the reduction current at -1.6V vs. SHE.

Gamry Cyclic Voltammetry Header Information

EXPLAIN
TAG CV
TITLE LABEL 500Cyclic Voltammetry Test Identifier
DATE LABEL 3/29/2024 Date
TIME LABEL 11:54:52 Time
NOTES NOTES 1 Notes...

PSTAT PSTAT IFC1010-20235 Potentiostat
VINIT POTEN -1.94000E-001 F Initial E (V)
VLIMIT1 POTEN -2.50000E+000 F Scan Limit 1 (V)
VLIMIT2 POTEN 2.00000E+000 F Scan Limit 2 (V)
VFINAL POTEN -1.94000E-001 F Final E (V)
SCANRATE QUANT 4.99999E+002 Scan Rate (mV/s)
STEPSIZE QUANT 1.00000E+000 Step Size (mV)
CYCLES IQUANT 3 Cycles (#)
IMODE SELECTOR 0 I/E Range Mode
IRANGE QUANT 1.37699E-002 Last Measured Current (A)
AREA QUANT 5.00000E+000 Sample Area (cm^2)
EQDELAY QUANT 5.00000E+000 Equil. Time (s)
IRCOMP SELECTOR 0 IRComp
PFCOR QUANT 5.00000E+001 PF Corr. (ohm)
SAMPLINGMODE SELECTOR 1 Sampling Mode
EOC QUANT 0 Open Circuit (V)
SEQUENCER TOGGLE TRUE Run as Sequence
PSTATMODEL IQUANT 64 Pstat Model
PSTATSECTION LABEL IFC1010-20235 Pstat Section
PSTATSERIALNO LABEL 20235 Pstat Serial Number
CTRLMODE IQUANT 1 Control Mode
ELECTROMETER IQUANT 0 RE=0 or CS=1
IESTAB IQUANT 2 I/E Stability
CASPEED IQUANT 4 Control Amp Speed
CONVENTION IQUANT 1 Current Convention
ICHRANGE IQUANT 2 Ich Range
ICHRANGEMODE TOGGLE F Ich Auto Range
ICHOFFSETENABLE TOGGLE F Ich Offset Enable
ICHOFFSET QUANT 0 Ich Offset (V)
ICHFILTER IQUANT 3 Ich Filter
VCHRANGE IQUANT 2 Vch Range
VCHRANGEMODE TOGGLE F Vch Auto Range
VCHOFFSETENABLE TOGGLE F Vch Offset Enable
VCHOFFSET QUANT 0 Vch Offset (V)
VCHFILTER IQUANT 3 Vch Filter
IERANGELOWERLIMIT IQUANT 4 I/E Range Lower Limit

IERANGEMODE	TOGGLE	T	I/E AutoRange
IERANGE	IQUANT	8	I/E Range
ACHSELECT	IQUANT	0	Ach Select
ACHRANGE	IQUANT	2	Ach Range
ACHOFFSETENABLE	TOGGLE	F	Ach Offset Enable
ACHOFFSET	QUANT	0	Ach Offset (V)
ACHFILTER	IQUANT	1	Ach Filter
SENSECABLEID	IQUANT	12	Sense Cable ID
PWRCABLEID	IQUANT	12	Power Cable ID
DCCALDATE	LABEL	1/11/2024	DC Calibration Date
ACCALDATE	LABEL	2/24/2018	AC Calibration Date
FRAMEWORKVERSION	QUANT	7.06	Framework Version
INSTRUMENTVERSION	LABEL	4.30	Instrument Version

Gamry Electro Impedance Spectroscopy Header Information

EXPLAIN			
TAG	EISPOT		
TITLE	LABEL	Potentiostatic EIS	Test Identifier
DATE	LABEL	3/29/2024	Date
TIME	LABEL	13:35:30	Time
NOTES	NOTES	1	Notes...

PSTAT	PSTAT	IFC1010-20235	Potentiostat
VDC	POTEN	0.00000E+000 T	DC Voltage (V)
FREQINIT	QUANT	2.00000E+004	Initial Freq. (Hz)
FREQFINAL	QUANT	2.00000E-001	Final Freq. (Hz)
PTSPERDEC	QUANT	1.00000E+001	Points/decade
VAC	QUANT	1.00000E+002	AC Voltage (mV rms)
AREA	QUANT	1.00000E+000	Sample Area (cm^2)
SPEED	SELECTOR	2	Optimize for:
ZGUESS	QUANT	1.00000E+002	Estimated Z (ohms)
EOC	QUANT	0	Open Circuit (V)
SEQUENCER	TOGGLE	TRUE	Run as Sequence
PSTATMODEL	IQUANT	64	Pstat Model
PSTATSECTION	LABEL	IFC1010-20235	Pstat Section
PSTATSERIALNO	LABEL	20235	Pstat Serial Number
CTRLMODE	IQUANT	1	Control Mode
ELECTROMETER	IQUANT	0	RE=0 or CS=1
IESTAB	IQUANT	0	I/E Stability
CASPEED	IQUANT	3	Control Amp Speed
CONVENTION	IQUANT	1	Current Convention
ICHRANGE	IQUANT	2	Ich Range
ICHRANGEMODE	TOGGLE	F	Ich Auto Range
ICHOFFSETENABLE	TOGGLE	T	Ich Offset Enable

ICHOFFSET	QUANT	0	Ich Offset (V)
ICHFILTER	IQUANT	4	Ich Filter
VCHRANGE	IQUANT	2	Vch Range
VCHRANGEMODE	TOGGLE	F	Vch Auto Range
VCHOFFSETENABLE	TOGGLE	T	Vch Offset Enable
VCHOFFSET	QUANT	0	Vch Offset (V)
VCHFILTER	IQUANT	4	Vch Filter
IERANGELOWERLIMIT	IQUANT	4	I/E Range Lower Limit
IERANGEMODE	TOGGLE	F	I/E AutoRange
IERANGE	IQUANT	11	I/E Range
ACHSELECT	IQUANT	0	Ach Select
ACHRANGE	IQUANT	2	Ach Range
ACHOFFSETENABLE	TOGGLE	F	Ach Offset Enable
ACHOFFSET	QUANT	0	Ach Offset (V)
ACHFILTER	IQUANT	1	Ach Filter
SENSECABLEID	IQUANT	12	Sense Cable ID
PWRCABLEID	IQUANT	12	Power Cable ID
DCCALDATE	LABEL	1/11/2024	DC Calibration Date
ACCALDATE	LABEL	2/24/2018	AC Calibration Date
FRAMEWORKVERSION	QUANT	7.06	Framework Version
INSTRUMENTVERSION	LABEL	4.30	Instrument Version

Gamry Pulse Electroplating Header Information

EXPLAIN			
TAG	REPEATING_CHRONOA		
TITLE	LABEL	Chronoamperometry Scan	Test Identifier
DATE	LABEL	3/29/2024	Date
TIME	LABEL	13:59:59	Time
NOTES	NOTES	1	Notes...

PSTAT	PSTAT	IFC1010-20235	Potentiostat
VSTEP1	POTEN	-1.97000E-001	F Step 1 Voltage (V)
TSTEP1	QUANT	1.00000E+000	Step 1 Time (s)
VSTEP2	POTEN	-2.00000E+000	F Step 2 Voltage (V)
TSTEP2	QUANT	1.00000E+001	Step 2 Time (s)
SAMPLETIME	QUANT	2.50000E-003	Sample Period (s)
DECIMATE	TOGGLE	F	Decimate
ILIMIT	QUANT	5.00000E+003	Limit I (mA/cm^2)
AREA	QUANT	1.00000E+001	Sample Area (cm^2)
IMODE	SELECTOR	0	I/E Range Mode
IRANGE	QUANT	1.00000E+003	Max Current (mA)
EQDELAY	QUANT	0.00000E+000	Equil. Time (s)
IRCOMP	SELECTOR	0	IRComp
PFCOR	QUANT	5.00000E+001	PF Corr. (ohm)

CYCLES IQUANT 2 Cycles (#)
SAMPLINGMODE SELECTOR 1 Sampling Mode
ELECTRODETYPE SELECTOR 0 Electrode Type
STRIPPING TOGGLE F Used for Stripping
POLARITY TOGGLE F Signal Polarity
LINEFREQ IQUANT 60 Line Frequency (Hz)
INTPERIOD QUANT NIL Integration Period (s)
SEQUENCER TOGGLE TRUE Run as Sequence
PSTATMODEL IQUANT 64 Pstat Model
PSTATSECTION LABEL IFC1010-20235 Pstat Section
PSTATSERIALNO LABEL 20235 Pstat Serial Number
CTRLMODE IQUANT 1 Control Mode
ELECTROMETER IQUANT 0 RE=0 or CS=1
IESTAB IQUANT 0 I/E Stability
CASPEED IQUANT 4 Control Amp Speed
CONVENTION IQUANT 1 Current Convention
ICHRANGE IQUANT 2 Ich Range
ICHRANGEMODE TOGGLE T Ich Auto Range
ICHOFFSETENABLE TOGGLE F Ich Offset Enable
ICHOFFSET QUANT 0 Ich Offset (V)
ICHFILTER IQUANT 3 Ich Filter
VCHRANGE IQUANT 3 Vch Range
VCHRANGEMODE TOGGLE T Vch Auto Range
VCHOFFSETENABLE TOGGLE F Vch Offset Enable
VCHOFFSET QUANT 0 Vch Offset (V)
VCHFILTER IQUANT 3 Vch Filter
IERANGELOWERLIMIT IQUANT 4 I/E Range Lower Limit
IERANGEMODE TOGGLE T I/E AutoRange
IERANGE IQUANT 12 I/E Range
ACHSELECT IQUANT 0 Ach Select
ACHRANGE IQUANT 2 Ach Range
ACHOFFSETENABLE TOGGLE F Ach Offset Enable
ACHOFFSET QUANT 0 Ach Offset (V)
ACHFILTER IQUANT 1 Ach Filter
SENSECABLEID IQUANT 12 Sense Cable ID
PWRCABLEID IQUANT 12 Power Cable ID
DCCALDATE LABEL 1/11/2024 DC Calibration Date
ACCALDATE LABEL 2/24/2018 AC Calibration Date
FRAMEWORKVERSION QUANT 7.06 Framework Version
INSTRUMENTVERSION LABEL 4.30 Instrument Version

Gamry Square Wave Header Information

EXPLAIN
TAG SQUARE_WAVE

TITLE	LABEL	Square Wave Voltammetry	Test Identifier
DATE	LABEL	3/29/2024	Date
TIME	LABEL	13:54:26	Time
NOTES	NOTES	1	Notes...

PSTAT	PSTAT	IFC1010-20235	Potentiostat
VINIT	QUANT	-1.97000E-001	Initial E (V)
VFINAL	QUANT	-2.75000E+000	Final E (V)
STEPSIZE	QUANT	2.00000E+000	Step Size (mV)
TIMERRES	QUANT	1.00000E-004	&Timer Resolution
FREQUENCY	QUANT	1.00000E+001	Frequency (Hz)
PULSESIZE	QUANT	1.00000E+002	Pulse Size E (mV)
PULSEON	QUANT	1.00000E-001	Pulse &Time (s)
NOISEREJECT	TOGGLE	T	Noise Rejection
AREA	QUANT	1.00000E+000	Sample Area (cm^2)
IMODE	SELECTOR	1	I/E Range Mode
IRANGE	QUANT	1.00000E+003	Max Current (mA)
EQDELAY	IQUANT	5	Equil. Time (s)
IRCOMP	SELECTOR	0	IRComp
PFCOR	QUANT	5.00000E+001	PF Corr. (ohm)
CYCLES	IQUANT	1278	C&ycles (#)
ELECTRODETYPE	SELECTOR	0	Electrode Type
STRIPPING	TOGGLE	F	Used for Stripping
POLARITY	TOGGLE	F	Signal Polarity
LINEFREQ	IQUANT	60	Line Frequency (Hz)
INTPERIOD	QUANT	0.0166667	Integration Period (s)
SEQUENCER	TOGGLE	TRUE	Run as Sequence
PSTATMODEL	IQUANT	64	Pstat Model
PSTATSECTION	LABEL	IFC1010-20235	Pstat Section
PSTATSERIALNO	LABEL	20235	Pstat Serial Number
CTRLMODE	IQUANT	1	Control Mode
ELECTROMETER	IQUANT	0	RE=0 or CS=1
IESTAB	IQUANT	2	I/E Stability
CASPEED	IQUANT	6	Control Amp Speed
CONVENTION	IQUANT	0	Current Convention
ICHRANGE	IQUANT	2	Ich Range
ICHRANGEMODE	TOGGLE	F	Ich Auto Range
ICHOFFSETENABLE	TOGGLE	F	Ich Offset Enable
ICHOFFSET	QUANT	0	Ich Offset (V)
ICHFILTER	IQUANT	3	Ich Filter
VCHRANGE	IQUANT	2	Vch Range
VCHRANGEMODE	TOGGLE	F	Vch Auto Range
VCHOFFSETENABLE	TOGGLE	F	Vch Offset Enable
VCHOFFSET	QUANT	0	Vch Offset (V)

```
VCHFILTER       IQUANT          3       Vch Filter
IERANGELOWERLIMIT IQUANT        4       I/E Range Lower Limit
IERANGEMODE         TOGGLE      F       I/E AutoRange
IERANGE         IQUANT          12      I/E Range
ACHSELECT       IQUANT          0       Ach Select
ACHRANGE        IQUANT          2       Ach Range
ACHOFFSETENABLE     TOGGLE      F       Ach Offset Enable
ACHOFFSET       QUANT           0       Ach Offset (V)
ACHFILTER       IQUANT          1       Ach Filter
SENSECABLEIDIQUANT              12      Sense Cable ID
PWRCABLEID  IQUANT              12      Power Cable ID
DCCALDATE       LABEL   1/11/2024       DC Calibration Date
ACCALDATE       LABEL   2/24/2018       AC Calibration Date
FRAMEWORKVERSION            QUANT           7.06    Framework Version
INSTRUMENTVERSION           LABEL   4.30    Instrument Version
```

Python Script for Automated Cyclic Voltammetry Batch Analysis

```
# -*- coding: utf-8 -*-
"""
Created on Tue Jan 21 19:18:46 2025

@author: Diana Horangic
"""
import os
import matplotlib.pyplot as plt
import numpy as np
from AUX_FUNCTIONS import *

Home = ".\DEMONSTRATION_DATASET"
Analytic_Integrals = True #Analytical integration
Data_Interval = (2.75, 0.3) #Voltage
Operator_Color = {"Chris" : 'red', "Steven" : 'green', "Kat" : 'blue'}

#There is also code written to run through a large file directory of data, and output
it to large excel documents or CSV files.
#It was written to output the analysis in columns labeled:
   #["TEMPERATURE", "DATE", "SCAN SPEED", "CURVE NUMBER", "V1 POINT", "V2
POINTS", "HALWAY DIP POINT", "AREA"]
#Examples are available with this demo, I have set aside some of those excel
spreadsheets.

if __name__ == "__main__":
   #1. Choose a compound - "TiCl", "ZrCl", "TiF" (technically tetra!)
   Compound = "TiCl"
   #2. Choose a range of CV scan rates (mV/sec) to look at, from 25 to 5k
```

```
    CV_Rates = ["25", "100", "500"]
    #3. Load the data from different operators.
    Operators = os.listdir(os.path.join(Home, Compound))
    print(f"The different people who took data with this compound are: {Operators}")
    #4. Either look at each scan, or run through the data taken for different operators.
    for op in Operators:
        file_directory = os.path.join(Home, Compound, op)
        file_locations = [os.path.join(file_directory, f"CV{CV}.txt") for CV in CV_Rates]
        for idx, file_ in enumerate(file_locations):
            CV = CV_Rates[idx]
            assert os.path.isfile(file_), f"The file path is {file_}"
            try:
                V, C, T = read_files(file_)
            except Exception as e:
                print(f"For file {file_}, error! {e}")
            V_s, C_s, T_s, Stored_Mins = process_curves(V, C, T, Data_Interval, file_)
            for curve_num in range(1, len(V_s)):
                minima, X, Y, list_, tolerance = condensed_analysis(V, C, V_s, C_s, curve_num,
Stored_Mins, CV, file_)

                plt.figure(figsize = (10,8))
                for tup_ in minima:
                    plt.axvline(x = X[tup_[0]], color='deeppink', linestyle = "--")
                    plt.axvline(x = X[tup_[1]], color='deeppink', linestyle = "--")
                plt.plot(X, Y, color=Operator_Color[op], label = f"Number of dips found by
preliminary analysis: {len(tup_)}", linewidth = 3.0)
                plt.xlabel("Voltage (V)")
                plt.ylabel("Current (A)")
                plt.title(f"Prelim. Analysis: Curve #{curve_num}, at scan speed {CV} mV/sec,
performed by operator {op} with compound {Compound}")
                plt.legend()
                plt.show()

                if len(list_) != 0:
                    plt.figure(figsize = (10,8))
                    range_ = 15
                    plt.plot(X, Y, color=Operator_Color[op], label = f"Number of dips found by
refined analysis: {len(list_)}", linewidth = 3.0)
                    for tup_ in list_:
                        idx_triplet, m, b, ab, cur, half1, half2, area = tup_
                        start, finish = idx_triplet[0], idx_triplet[1] + range_
                        C_fit = (X[start : finish] * m) + b
                        C_original = Y[start : finish]
                        plt.axvline(x = ab[0], color='deeppink', linestyle = "--")
                        plt.axvline(x = ab[1], color='deeppink', linestyle = "--")
                        plt.plot(X[start : finish], C_fit, color = 'black', linestyle = ':')
```

```
                between_ = int ( (float( (start) + (finish)) / 2.0)  )
                xmax = X[between_]
                ymax = Y[between_]
                x2 = X[between_] #- 0.15 * np.max(X[start:finish])
                y2 = Y[between_] - 0.15 * np.max(C_original)
                C_fit_half = C_fit[int( float(len(C_fit)) / 2.0)]
                C_org_half = C_original[int( float(len(C_fit)) / 2.0)]
                bool_valid_area = True
                if C_org_half > C_fit_half or abs(C_org_half - C_fit_half) <= tolerance:
                   bool_valid_area = False
                sci_area = f"{area:.4e}"
                plt.annotate(f'{bool_valid_area}', xy=(xmax, ymax), xytext=(xmax,
ymax),
                             bbox=dict(boxstyle='square', fc='white', ec='black'),
                             arrowprops=dict(facecolor='black', arrowstyle='-'))
                plt.annotate(f'{sci_area}', xy=(x2, y2), xytext=(x2, y2),
                             bbox=dict(boxstyle='square', fc='white', ec='black'),
                             arrowprops=dict(facecolor='black', arrowstyle='-'))
            plt.xlabel("Voltage (V)")
            plt.ylabel("Current (A)")
            plt.title(f"Refined Analysis: Curve #{curve_num}, at scan speed {CV}
mV/sec, performed by operator {op} with compound {Compound}")
            plt.legend()
            plt.show()
```

CV Data Analysis

Data Organization

Data is organized by 1) different operators, and 2) date of data acquisition. The program reads each operator folder and each date folder, then reads a separate text file for each scan speed (e.g. 10 mV/sec, 50 mV/sec, *etc.*). If the file does not exist in that directory, it is skipped. There is a global dictionary containing the concentration, ion, temperature, and duration of each run that the user defines.

Data Reading and Curve Separation

Text files are read line by line. There is a title in the text file that signals the beginning of all data being taken. After getting the first line of real data, the program cycles through every subsequent line searching for a line that starts with either "Pt" or “CURVE”. This indicates a new run of data and in this line is also either a 2, 3, or 4, which gives the number of the run. The indices dividing each curve are stored. All values of current, voltage, temperature, and time are stored subsequently in a list of rows. This list is converted into a Pandas.DataFrame and stored. Then, the rows of voltage, current, and time are converted to NumPy arrays. A list containing each concatenated NumPy array for each curve is made using the stored indices to divide the one long array into each curve. This is done for voltage, current, and time.

Data Preprocessing

Analysis of trials of scan speed at or above 2000 mV/sec did not yield stable results, as the response of the system (and therefore the analysis) was erratic (i.e., ~1000 mV/s is the max diffusion point of the system). Voltage and current data are shifted for analysis such that both are positive for every point. The order of the array naturally runs "backward" from a higher voltage to a lower voltage; this is reversed by adding the absolute value of the minimum value of each array to every point in the array. These minima are stored and used to convert voltage and current points back to their original value later. The runs are trimmed to run from the minimum to the maximum voltage of the run.

Second Derivative and Maxima, Minima, and Inflection Points Calculation

There is a loop that goes over each curve. The first curve is cut out and never analyzed as it was performed to stabilize the signals from the electrochemical cell. In the loop, voltage and current arrays are stored as X and Y respectively. In preparation for numerical differentiation, the variable dX is calculated where $dX = X[1] - X[0]$. This is the initial "step" of the voltage array used to initialize the process. Multiple derivatives of the data are used to find the start and end of each reduction dip. The start and end of each dip are stored in an array for processing.

Linear Fitting

The pairs of reduction dip start and end indices (i_{start}, i_{end}) are fed to a linear fitting function. These indices are used to generate two pairs of voltage and current. These are the pairs used to generate a line. The slope and intercept are returned by this function and stored for every reduction dip pair.

Integration of Reduction Dips

Integration of each reduction dip is performed using the index pairs, the slope, and the intercept generated before the reduction dip. A numeric integration of the real data is performed using SciPy trapz function. Before the current is integrated, a Gaussian filter with a standard deviation of 4.0 is applied to it. The integration of the line generated by the start and end voltage of the reduction dip is performed analytically. The integral of the line is subtracted from the integral of the original data and stored as the reduction dip area. The start, end, and halfway voltages of each reduction peak are also stored in their original value. They are converted back using the stored minima mentioned in the Data Preprocessing section.

Data Storage

There are two methods of data storage. The first is to store everything in a long CSV file with a row marking the scan speed. The software generates a separate CSV for each operator. The second method creates an Excel file for each operator. This file has a sheet for every scan speed the operator collected data for, and all dates and the temperature of the run are included in each sheet. It is a condensed Excel file containing the averages of trials performed under the same experimental conditions. It can also include the standard deviation and standard error if specified by the user.